

Neutron Scattering Studies of LiCoPO_4 & LiMnPO_4

Wei Tian,¹ Jiying Li,^{2,3} Haifeng Li,¹ Jeffrey W. Lynn,² Jerel L. Zarestky,¹ and David Vaknin¹

¹Ames Laboratory and Department of Physics and Astronomy, Iowa State University, Ames, Iowa 50011, USA

²NCNR, National Institute of Standards and Technology, Gaithersburg, MD 20899, USA

³Department of Materials Science and Engineering,
University of Maryland, College Park, MD 20742, USA

LiCoPO_4 ($T_N \approx 21.8$ K) & LiMnPO_4 ($T_N \approx 34$ K) are antiferromagnetic insulators exhibiting large magnetoelectric effects. We performed inelastic neutron scattering (INS) experiments to investigate the spin dynamics of these systems and analyzed the measured magnetic spectra by linear spin-wave theory, taking into account intra- and inter-plane nearest, next nearest neighbor magnetic exchange interactions and single ion anisotropy. The INS results indicate that LiMnPO_4 behaves like a quasi-2D material and that the single ion anisotropy in LiCoPO_4 is comparable to the nearest-neighbor magnetic exchange interaction rendering Ising-type behavior of LiCoPO_4 . Neutron diffraction studies of LiMnPO_4 in applied magnetic fields reveal a spin-flop transition at ~ 3.5 Tesla with characteristics of a second order phase transition.

I. INTRODUCTION

LiCoPO_4 and LiMnPO_4 are antiferromagnetic (AFM) insulators belonging to the olivine family of lithium orthophosphates LiMPO_4 ($M = \text{Mn}^{2+}$, Fe^{2+} , Co^{2+} , Ni^{2+})^{1,2}. These materials are known for their exceptionally large magnetoelectric (ME) effect^{3,4}. To date, it remains an open question whether the ME effects of LiMPO_4 are intrinsic due to the particular local environment surrounding the transition metal ions or due to domain formation structures. The recent observations of weak ferromagnetism⁵, ME “butterfly loop” anomaly⁶, and in particular the ferrotoroidic domain structure in LiCoPO_4 ⁷ have ignited renewed interest in these materials^{8–12}.

LiCoPO_4 and LiMnPO_4 crystallize in the orthorhombic crystal structure, space group $Pnma$ (no. 62) at room temperature. As illustrated in Fig. 1 where only the P and M^{2+} ($M = \text{Co}$, Mn) ions are shown for clarity, the magnetic M^{2+} ($S = 3/2$ for Co^{2+} and $S = 5/2$ for Mn^{2+}) ions are at the center of a slightly distorted MO_6 octahedron that share oxygen anion with PO_4 tetrahedral forming buckled MO layers stacking along the a -axis. LiCoPO_4 ($T_N \approx 21.8$ K) and LiMnPO_4 ($T_N \approx 34$ K) undergo long range AFM transitions with a collinear AFM ground state. They adopt the same magnetic structure ($Pnm'a$) differing only in spin orientation. The spins are oriented along the b -axis for LiCoPO_4 and along the a -axis for LiMnPO_4 ^{2,8}. As depicted in Fig. 1, the magnetic coupling in the layer is through the M-O-M super-exchange interactions, and the coupling between adjacent layers is mediated through the PO_4 phosphate group, rendering the magnetic system quasi-two-dimensional. We have recently reported inelastic neutron scattering (INS) studies and determined the microscopic magnetic interactions in these two systems (the detailed results have been published in Ref. 13 and Ref. 14). In this manuscript, we briefly present the main INS results and preliminary neutron diffraction measurements under applied magnetic field ($H \parallel a$ -axis) of LiMnPO_4

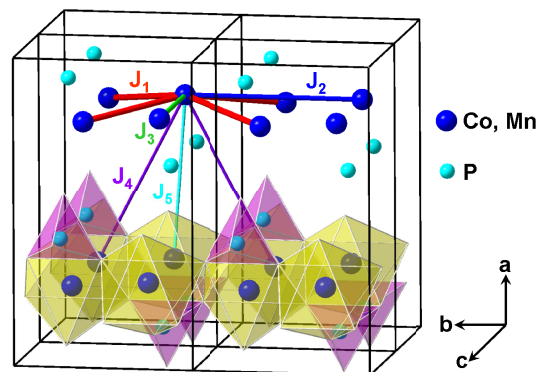


FIG. 1: (Color online) Schematic crystal structure of LiMPO_4 ($M = \text{Co}$, Mn). The P and M^{2+} magnetic ions are shown, and only one layer of the MO_6 octahedrons and PO_4 tetrahedrons is illustrated for clarity. The in-plane nearest-neighbor (J_1), next-nearest-neighbor (J_2 , J_3), and inter-plane nearest, next-nearest-neighbor (J_4 , J_5) magnetic exchange interactions included in the spin wave theory are labeled.

that reveal a spin-flop transition at ~ 3.5 Tesla.

II. EXPERIMENTAL TECHNIQUES

Neutron scattering experiments were carried out using single crystal samples grown by the standard LiCl flux method similar to that reported in Ref. 11,15. The crystals were characterized by X-ray diffraction measurements and no impurity phases were detected. Inelastic neutron scattering measurements of LiCoPO_4 and LiMnPO_4 were performed on the HB1A triple-axis spectrometer (TAS) at HFIR, the BT7, BT9 and SPINS TAS spectrometers at NIST. The neutron diffraction measurements of LiMnPO_4 in applied magnetic fields were performed on the BT7 TAS employing a 11 Tesla vertical magnet with the crystal oriented in the $(0\ K\ L)$ scattering plane and the magnetic field applied along the a -axis, $H \parallel a$. All measurement results have been normalized to

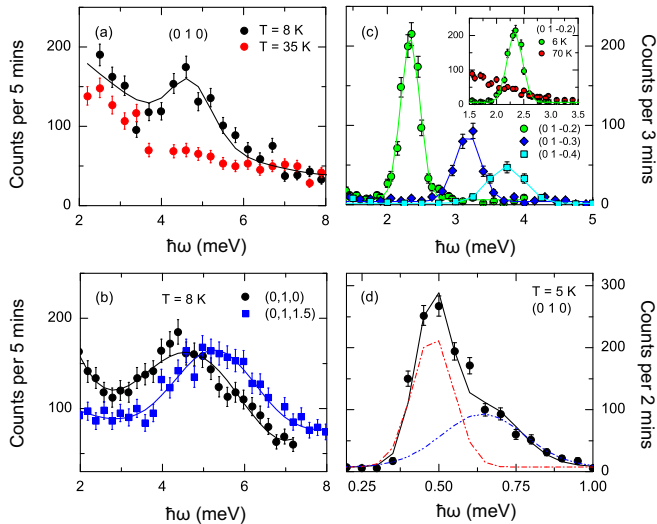


FIG. 2: (Color online) Representative constant wave-vector scans of LiCoPO₄ and LiMnPO₄. (a) The ~ 4.7 meV excitation observed in LiCoPO₄ measured at (0 1 0) at $T = 8$ K and 35 K. (b) Weak dispersion observed in LiCoPO₄ comparing constant wave-vector scans measured along the L direction at $T = 8$ K. (c) LiMnPO₄ constant wave-vector scans measured along the L direction at $T = 6$ K. (d) LiMnPO₄ constant wave-vector scan measured at the zone center indicates two energy gaps. Intensities were normalized to the incident neutron flux by counting against neutron monitor counts.

a beam monitor count.

III. RESULTS AND DISCUSSIONS

Figure. 2 shows representative constant wave-vector scans of LiCoPO₄ (Fig. 2 (a)-(b)) and LiMnPO₄ (Fig. 2 (c)-(d)) (error bars in this paper are statistical in origin and represent one standard deviation). As shown in Fig. 2 (a), a single excitation of $\hbar\omega \approx 4.7$ meV is detected at $T = 8$ K in the fully ordered phase of LiCoPO₄. At a temperature well above T_N ($T = 35$ K) the peak intensity is significantly reduced demonstrating the excitation is magnetic in origin. Fig. 2 (b) compares constant wave-vector scans measured at (0 1 0) and (0 1 1.5), which typically correspond to the minimum and maximum spin wave excitations along the L direction. The ~ 4.7 meV excitation at (0 1 0) shifts to higher energy transfer, ~ 5.3 meV at (0 1 1.5) indicating weak dispersion along the L direction. Measurements along the (H 1 0) and (0 K 0) directions indicate the ~ 4.7 meV excitation propagating weakly along both the H and K directions as well. For LiMnPO₄, Fig 2 (c) compares constant wave-vector scans measured along (0 1 L) demonstrating the magnetic excitation observed in LiMnPO₄ propagating strongly along the L direction in contrast with LiCoPO₄. In particular, as shown in Fig. 2 (d), two energy gaps (~ 0.48 meV and ~ 0.64 meV) were observed for LiMnPO₄ at the zone center (measurements conducted on SPINS).

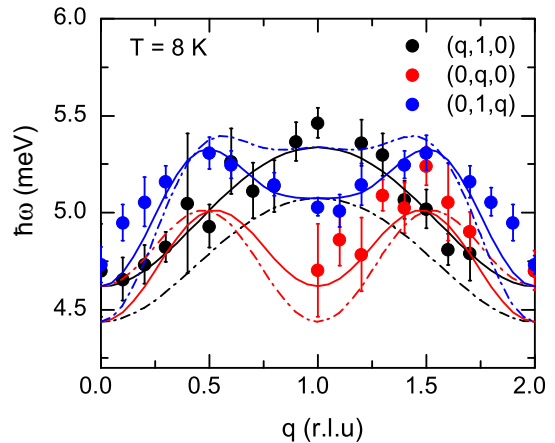


FIG. 3: (Color online) LiCoPO₄ spin-wave dispersion curves along three reciprocal directions constructed from a series of constant wave-vector scans. Data points are obtained based upon a Gaussian peak approximation. The solid and dashed lines are calculations based upon a global fit to the linear spin wave approximation theory as described in the text.

Based on a series of constant wave-vector energy-scans below T_N , we compile the spin wave dispersion curves in Figs. 3 and 4 for LiCoPO₄ and LiMnPO₄, respectively. As shown in Fig. 4, the dispersion of LiMnPO₄ along the H direction is relatively weak compared to the ones along the K and L directions suggesting stronger coupling in the bc -plane consistent with the layered magnetic structure of LiMnPO₄. On the other hand, as shown in Fig. 3, weak dispersion was observed in LiCoPO₄ with a band width less than 1 meV exhibiting Ising-type behavior. The large uncertainties in the LiCoPO₄ experimental data are associated with the instrument resolution of thermal neutron triple-axis spectrometers, the energy resolution is $\Delta E \sim 1$ meV at the elastic position. The large experimental uncertainty has a significant effect in the theoretical modeling of LiCoPO₄.

The obtained spin wave dispersion curves are analyzed in the linear spin wave theory framework. The proposed spin Hamiltonian^{16,17} taking into account different magnetic exchange interactions (J_1 to J_5 in Fig. 1) can be written by the following equation:

$$\mathcal{H} = \sum_{i,j} J_{ij} \mathbf{S}_i \cdot \mathbf{S}_j + \sum_{i,\alpha} D_\alpha (S_i^\alpha)^2, \quad (1)$$

where D_α ($\alpha = x, y, z$) represents the single-ion anisotropy along the x , y , and z -directions. Within the linear spin wave approximation, the derived spin wave dispersion from Eq. (1) is given by:

$$\hbar\omega = \sqrt{A^2 - (B \pm C)^2}. \quad (2)$$

The definition of parameters A, B and C in Eq. (2) is described in Ref.13 and Ref.14 for LiCoPO₄ and LiMnPO₄ respectively. The $(B \pm C)$ in Eq. (2) indicates that there are two non-degenerate spin wave branches due to the different values of D_x and D_y .

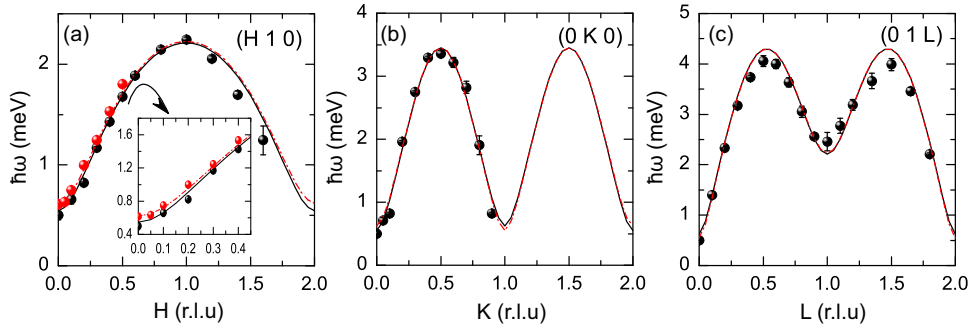


FIG. 4: (Color online) Spin-wave dispersion curves of LiMnPO_4 along three reciprocal directions constructed from a series of constant wave-vector scans measured at $T = 6$ K. Data points are obtained based upon a Gaussian peak approximation. The solid and dashed lines are calculations based upon a global fit to the linear spin wave approximation theory as described in the text. The inset in (a) shows the two spin wave branches observed using SPINS high resolution triple-axis spectrometer.

The magnetic spectra of LiMnPO_4 can be adequately described by the proposed spin-wave model. The non-linear least squares fit obtained for the LiMnPO_4 magnetic spectra using Eq. (2) (“B-C” branch) yields the following parameter values: $J_1 = 0.48 \pm 0.05$ meV, $J_2 = 0.2 \pm 0.038$ meV, $J_3 = 0.076 \pm 0.004$ meV, $J_4 = 0.036 \pm 0.002$ meV, $J_5 = 0.062 \pm 0.003$ meV, $D_x = 0.0069 \pm 0.001$ meV and $D_y = 0.0089 \pm 0.001$ meV. The calculated dispersion curves using the obtained fitting parameter values are plotted in Figure. 4, solid lines for the “B-C” branch and dashed lines for the “B+C” branch, respectively. As shown in Fig. 4, the calculated two spin wave branches almost overlap with ~ 0.1 meV separation at the zone center consistent with the two excitations observed at the zone center as shown in Fig. 2 (d). The inset in Fig. 4 (a) indicates that the calculated second branch agrees well with the SPINS data where two excitations can be resolved. The obtained inter-plane couplings (J_4 , J_5) are much weaker compared to the strongest intra-plane interaction J_1 indicating that LiMnPO_4 is magnetic quasi-2D as expected by its layered magnetic structure. The intra-plane coupling J_2 and J_3 have the same sign as J_1 suggesting that they compete with J_1 giving rise to strong critical scattering. The obtained single ion anisotropies D_x and D_y are very weak indicating that a spin-flop transition can occur under the influence of applied magnetic field. The detailed account of this study is given in Ref. 14.

Similarly, fitting the spin-wave dispersions expressed by Eq. (2) to the observed magnetic spectra of LiCoPO_4 yields: $J_1 = 0.771 \pm 0.144$ meV, $J_2 = 0.129 \pm 0.113$ meV, $J_3 = 0.208 \pm 0.102$ meV, $J_4 = -0.167 \pm 0.067$ meV, $J_5 = -0.193 \pm 0.102$ meV, $D_x = 0.73 \pm 0.15$ meV, $D_y = 0.808 \pm 0.159$ meV. The solid and dashed lines in Fig. 3 are the calculations of the two spin wave branches using the obtained parameters. It is remarkable that large single-ion anisotropy was obtained that is comparable to the strongest nearest-neighbor magnetic interaction J_1 , $D_x \sim D_y \sim J_1$. Such relatively strong anisotropy may split the $S = 3/2$ quartet of the Co^{2+} ion into two doublets rendering the suggested Ising-type charac-

ter to LiCoPO_4 ⁹. Our studies indicate that single ion anisotropy plays an important role in the spin dynamics of LiCoPO_4 . As shown in Fig. 3, the calculated spin wave dispersion predicts a maximum separation of ~ 0.3 meV at (0 1 0). Both thermal neutron TAS data (with a resolution of ~ 1 meV) and cold neutron SPINS high resolution data (with a resolution of ~ 0.28 meV) show only one excitation around ~ 4.7 meV. In our measurements, we could not resolve the two branches. It is possible that the second excitation is very weak in intensity since the model does not predict intensities. Another possibility is that the intrinsic linewidth of the observed excitations are broader than the resolution (~ 1 meV) suggesting contributions from both branches overlap and cause the broadening. Detailed studies together with the observation of an anomalous low energy magnetic excitation are reported in Ref. 13.

Neutron diffraction measurements of LiMnPO_4 in magnetic field reveal a spin-flop transition at ~ 3.5 Tesla. Fig. 5 shows typical scans monitoring the (0 1 0) and (0 0 1) strong magnetic reflections as a function of applied magnetic field. The magnetic field was applied along the moment direction, $H \parallel a$ -axis. The data of (0 0 1) (Fig. 5 (a)) at 2 K shows that the peak intensity of (0 0 1) disappears above $H_c \sim 3.5$ Tesla indicating a spin-flop transition, we refer to H_c as the critical field associate with the spin-flop transition. On the other hand, as shown in Fig. 5 (b), the peak intensity of (0 1 0) remains nearly the same at fields both above and below H_c . For magnetic scattering, only those spin components which are perpendicular to the scattering vector have non-vanishing cross-section. Hence the disappearance of the (0 0 1) peak, and the nearly unchanged (0 1 0) peak indicate that the flopped spins are aligned nearly along the c -axis above H_c . As depicted in the inset in Fig. 5(a), no hysteresis is observed upon increasing and decreasing the applied magnetic field through the transition indicating this may be a second order phase transition. An anomalous dip is observed in the (0 1 0) field scan (Fig. 5 (b)) suggesting the existence of an intermediate phase with the critical field H_c extending

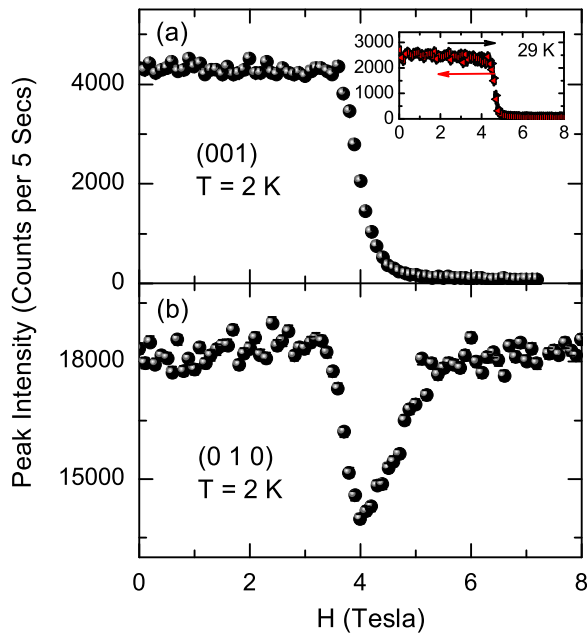


FIG. 5: (Color online) Magnetic field induced spin-flop transition in LiMnPO_4 , the magnetic field was applied along the a -axis, $H \parallel a$. (a) $(0\ 0\ 1)$ peak intensity vs. H at 2 K. Inset: $(0\ 0\ 1)$ peak intensity measured with increasing and decreasing H at 29 K. (b) $(0\ 1\ 0)$ peak intensity vs. H at 2 K.

over a range of ~ 1.6 Tesla at 2 K. We derived the magnetic field versus temperature phase diagram based on field and temperature dependent neutron diffraction and magnetization measurements. The phase diagram and detailed data analysis of this spin-flop transition will be reported elsewhere¹⁸. Our preliminary results of the characteristics of the spin-flop transition suggest the existence of anisotropic magnetic exchange that competes with the single ion anisotropy.

Acknowledgments

Ames Laboratory is supported by the U. S. Department of Energy Office of Basic Energy Science under Contract No. DE-AC02-07CH11358. The HFIR is a national user facility funded by the United States Department of Energy, Office of Basic Energy Sciences, Materials Science, under Contract No. DE-AC05-00OR22725 with UT-Battelle, LLC. The work has benefited from the use of the NIST Center of Neutron Research at the National Institute of Standards Technology, where SPINS is supported in part by the National Science Foundation under Agreement No. DMR-0454672.

- ¹ H. D. Megaw, *Crystal Structure - A working Approach* (Saunders Philadelphia, 1973) p. 249.
- ² R. P. Santoro, R. E. Newnham, and S. Nomura, *J. Phys. Chem. Solids* **27**, 655 (1966); P. Santoro, D. J. Segal, and R. E. Newnham, *J. Phys. Chem. Solids* **27**, 1192 (1966); R. P. Santoro and R.E. Newnham, *Acta Crystallogr.* **22**, 344 (1967).
- ³ M. Mercier, J. Gareyte, and E. F. Bertaut, *C. R. Acad. Sci. Paris B* **264**, 979 (1967); M. Mercier, *Rev. Gen. Electr.* **80**, 143 (1971).
- ⁴ J.-P. Rivera, *Ferroelectrics* **161**, 147 (1994).
- ⁵ Yu. Kharchenko, N. Kharchenko, M. Baran, and R. Szymczak, *cond-mat: 0310156*.
- ⁶ I. Kornev, M. Bichurin, J.-P. Rivera, S. Gentil, H. Schmid, A. G. M. Jansen, and P. Wyder, *Phys. Rev. B* **62**, 12247(2000).
- ⁷ B. B. van Aken, J.-P. Rivera, H. Schmid, and M. Fiebig, *Nature* **449**, 702 (2007).
- ⁸ D. Vaknin, J. L. Zarestky, J. E. Ostenson, B. C. Chakoumakos, A. Gofñi, P. J. Pagliuso, T. Rojo, and G. E. Barberis, *Phys. Rev. B* **60**, 1100 (1999).
- ⁹ D. Vaknin, J. L. Zarestky, L. L. Miller, J.-p. Rivera, and H. Schmid, *Phys. Rev. B* **64** 224414 (2002).
- ¹⁰ D. Vaknin, J. L. Zarestky, J.-P. Rivera, and H. Schmid, *Phys. Rev. Lett.* **92**, 207201 (2004).
- ¹¹ J. Li, V. O. Garlea, J. L. Zarestky, and D. Vaknin, *Phys. Rev. B* **73**, 024410 (2006).
- ¹² T. B. S. Jensen, N. B. Christensen, M. Kenzelmann, H. M. Rønnow, C. Niedermayer, N. H. Andersen, K. Lefmann, J. Schefer, M. v. Zimmermann, J. Li, J. L. Zarestky, and D. Vaknin, *Phys. Rev. B* **79**, 092412 (2009).
- ¹³ Wei Tian, Jiying Li, Jeffrey W. Lynn, Jerel L. Zarestky, and David Vaknin, *Phys. Rev. B* **78**, 184429 (2008).
- ¹⁴ Jiying Li, Wei Tian, Ying Chen, Jerel L. Zarestky, Jeffrey W. Lynn, and David Vaknin, *Phys. Rev. B* **79**, 144410 (2009).
- ¹⁵ V. I. Fomin, V. P. Genezdilov, V. S. Kurnosov, A. V. Peschanskii, A. V. Yeremenko, H. Schmid, J.-P. Rivera, and S. Gentil, *Low Temp. Phys.* **28**, 203 (2002).
- ¹⁶ T. B. S. Jensen, N. B. Christensen, M. Kenzelmann, H. M. Rønnow, C. Niedermayer, N. H. Andersen, K. Lefmann, M. Jiménez-Ruiz, F. Demmel, J. Li, J. L. Zarestky, and D. Vaknin, *Phys. Rev. B*, **79**, 092413 (2009).
- ¹⁷ T. B. S. Jensen, Ph. D. Thesis, Risø DTU and University of Copenhagen (2007), <http://www.bricksite.com/tstibius>.
- ¹⁸ Haifeng Li *et al*, in preparation.